Received: 30 August 2018 | Accepted: 13 December 2018 | Published on: 25 March 2019

DOI: 10.1002/asna.201913614

ORIGINAL ARTICLE

Astronomische Nachrichten

Simultaneous Kepler/K2 and XMM-Newton observations of superflares in the Pleiades

M. G. Guarcello[1,*] | C. Argiroffi[1,2] | J. J. Drake[3] | E. Flaccomio[1] | J. López-Santiago[4] | G. Micela[1] | F. Reale[1,2] | L. Rebull[5,6] | S. Sciortino[1] | J. Stauffer[6] | V. Antoniou[3] | J. D. Alvarado-Gomez[3]

[1]INAF, Osservatorio Astronomico di Palermo, Palermo, Italy
[2]Dipartimento di Fisica e Chimica, Universitá di Palermo, Palermo, Italy
[3]High Energy Astrophysics Division, Harvard-Smithsonian Center for Astrophysics, Cambridge, Massachusetts
[4]Departamento de Astrofísica y Ciencias de la Atmósfera, Universidad Complutense de Madrid, Madrid, Spain
[5]Infrared Science Archive (IRSA), Infrared Processing and Analysis Center (IPAC), California Institute of Technology, Pasadena, California,
[6]Spitzer Science Center (SSC), Infrared Processing and Analysis Center (IPAC), California Institute of Technology, Pasadena, California,

***Correspondence**
M. G. Guarcello, INAF, Osservatorio Astronomico di Palermo, Piazza del Parlamento 1, Palermo 90134, Italy.
Email: mario.guarcello@inaf.it

Together with coronal mass ejection, flares are the most energetic stellar magnetic events, ignited by a sudden release of magnetic energy, which triggers a cascade of interconnected phenomena, each resulting in emission in different bands. For this reason, flares are intrinsic multiwavelength phenomena. In particular, optical and soft X-ray emission probes two different events occurring during flares: the heating of plasma in the upper photosphere at the footpoints of the magnetic loops and the heating and cooling of the plasma confined in the loops in the corona, respectively. To characterize powerful flares observed in optical and X-rays, constrain the energy released in both bands, the geometry of the loops, and to study flares time evolution, we studied the brightest flares occurred in the 125-Myr-old stars in the Pleiades observed simultaneously with x-ray multi-mirror mission/Newton and Kepler/K2.

KEYWORD
stars: activity – stars: coronae – stars: flare – X-rays: stars

1 | INTRODUCTION

Stellar flares are powerful phenomena due to the interaction between stellar magnetic field and plasma. Following the standard model (Fletcher et al. 2011), during flares, a large amount of energy previously stored in the magnetic field is released, accelerating a flow of high-speed electrons up to MeV energies. This energy is deposited on the underlying dense chromosphere at the loop footpoints, heating the surrounding plasma to 10 or more million degrees. Very quickly, the pressure in the heated plasma exceeds the ambient chromospheric pressure making the heated plasma expand and fill the magnetic tube above.

Flares are intrinsic multiwavelength phenomena, releasing energy in several bands of the electromagnetic spectrum (Benz 2008). Although technically challenging, multiwavelength observations of flares occurring in stars with different properties are thus required to fully understand the physics of flares and whether it changes during stellar evolution.

To study flares occurring in stars more active than the Sun in optical and X-rays, we obtained new XMM/Newton observations of the Pleiades during the Kepler K2 Campaign 4 observations. Given their proximity to the Sun (134 ± 6 pc, Gaia Collaboration et al. 2016), young age (125 Myrs, Stauffer et al. 1998), and rich population (with 2107 stars with high probability of being members identified by Bouy et al. 2015), the Pleiades represent a perfect target to study stellar variability over a wide range of stellar masses.

2 | ANALYZED DATA

The Pleiades have been included in the Kepler/K2 Campaign 4 and observed from February 8, 2015 to April 20, 2015, providing light curves for a total of 1020 high probability Pleiades members. We analyzed K2 light curves in the long-cadence mode (time resolution of ∼30 min). We also analyzed six X-ray observations of the Pleiades obtained

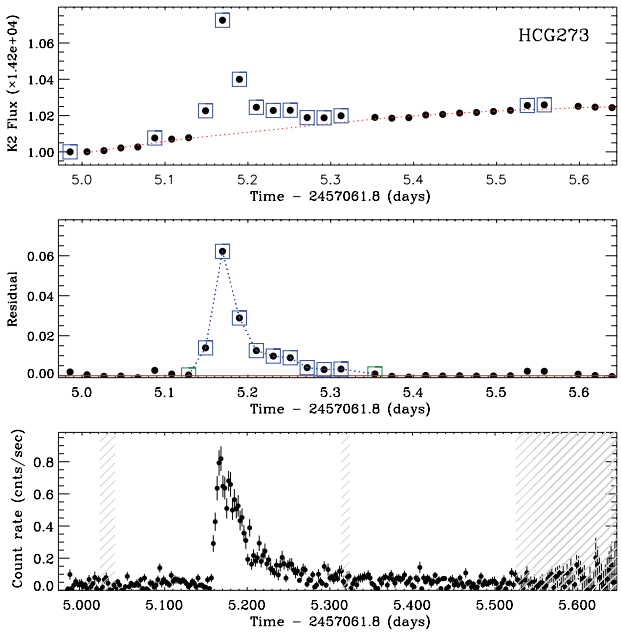

FIGURE 1 Light curves of HCG 273. Top panel: K2 light curve. The error bars of the K2 data points are smaller than the plot symbols. The red dotted line marks the polynomial used to fit the quiescent light curve; the blue squares mark the points corresponding to the flare. Central panel: residuals of the K2 light curve from the best fit polynomial function. The green squares mark the K2 point observed just before and after the flare. Bottom panel: The combined background-subtracted MOS + PN X-ray light curve. Shaded regions are "bad time intervals" in at least one EPIC detector

on February 2015 10th, 11th, 13rd, 17th, 18th, and 26th with XMM-Newton using the EPIC camera. Images were processed using SAS v.15 adopting the standard pipeline.

3 | OBSERVED FLARES AND THE STELLAR SAMPLE

The detection of the X-ray sources in the XMM images was performed with the wavelet convolution code PWXDetect (Damiani et al. 1997a, 1997b). We then extracted the X-ray light curves of all detected sources following the prescription of the SAS guide.

We selected X-ray flares in the combined MOS + PN light curves using the Maximum Likelihood method (Albacete Colombo et al. 2007; Caramazza et al. 2007; Scargle 1982). We then visually inspected the K2 light curves of the stars where X-ray flares occurred selecting 12 objects with bright flares observed both in optical and X-rays. All these stars are bona fide cluster members, with membership probability approaching unity as obtained by Bouy et al. (2013), and with the effective temperatures ranging from 3135 K to 6219 K. We calculated their luminosity in the Kepler band in quiescence ($L_{kep,quies}$) from their magnitude in the Kepler band.

Figure 1 shows the K2 and XMM light curves of one star in our sample (HCG 273). To define the quiescent level, we performed a fit of the portion of the K2 light curve during the XMM observations with a polynomial of the fifth order.

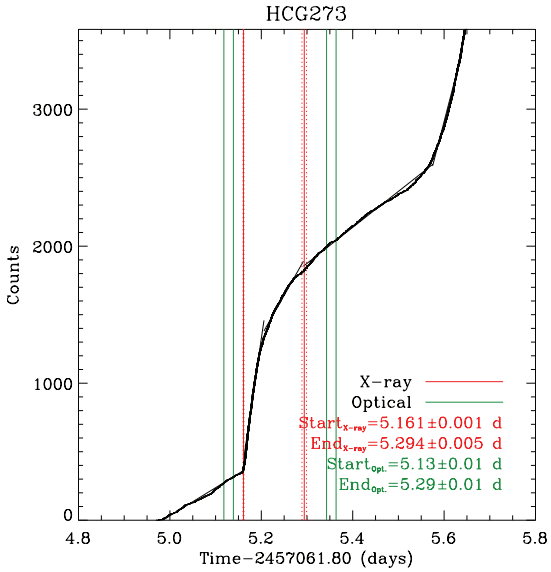

FIGURE 2 Sequence of arrival time of the detected X-ray broad band photons for HCG 273. The green lines mark the start and end time of the optical flare (in both cases the 1σ range centered on the nominal value adopting a 15 min uncertainty). Red lines delimit the X-ray flare (the solid line mark the nominal value, the dotted lines delimit the $\pm 1\sigma$ range)

3.1 | Flare durations

We calculated flare durations in the K2 light curves as the difference between the central time of the bins just before and after the flares, that is, those marked with green squares in Figure 1, with an adopted uncertainty of $15 \times \sqrt{2} = 21.2$ min. In the XMM light curves, the background brightness and variability prevented us from adopting the same approach. We thus estimated the duration of the X-ray flares directly from the arrival sequence of detected photons, as shown in Figure 2. This figure shows the detection sequence of all the X-ray photons in the broad band for the star HCG 273. To isolate the quiescence from the flare and thus derive its start and end times, we defined in each of these sequences the time intervals characterized by an almost constant count rate using K-S tests to compare the observed sequence with that expected from a linear relation. The intervals containing the flares are thus easily recognized given their larger slope compared with those containing quiescent emission. In eight cases, the optical flare onset preceded that of the X-ray flare, while the opposite occurred only in one case (HCG 150). This is compatible with the general model of flares with the optical event in the chromosphere/upper photosphere preceding the X-ray flare in the magnetic loop.

Figure 3 compares the duration of the flares in optical and X-rays. To account for the small number of data points in the scatter plot in this figure, we have performed six linear fits, adopting different algorithms for the linear regression, using the *IDL* routine *SIXLIN*. The resulting slopes are shown in the bottom right corner of the figure, and they typically are slightly smaller than one. This indicates that optical and X-ray flare duration is similar even if typically slightly longer in X-rays, as observed in most of solar flares.

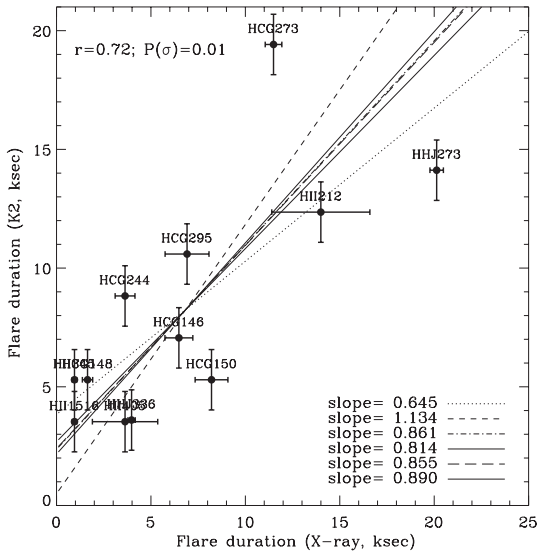

FIGURE 3 Flares duration in optical vs. X-rays. For each data point, we show the name of the star. The lines mark six linear fits performed with the *IDL* routine *SIXLIN*. The resulting slopes are indicated in the bottom right corner. In the top left corner we also show the Spearman's rank correlation coefficient and the significance of its deviation from zero

Figure 4 shows flare durations in optical and X-rays as a function of stellar rotation period. Rotation periods were calculated from K2 light curves by Rebull et al. (2016). In both bands, we observed a correlation between the duration of the flares and the rotation period. This correlation may indicate that rapidly rotating stars predominantly host short flares. Because short flares typically indicate small flaring structures, and probably short magnetic loops, this might be in general agreement with the scenario that in rapidly rotating stars the intense centrifugal stripping inhibits the formation of long loops and reduces the volume available for stellar coronae (Argiroffi et al. 2016). However, a larger and more complete sample of flares would be necessary to finally assess if a correlation between flare duration and stellar rotation exists.

4 | TIME-AVERAGED PROPERTIES

We computed the energy released during the optical flares in the Kepler band ($E_{kep,flare}$) from the Equivalent duration (ED) of each flare: $E_{kep,flare} = ED \times L_{kep,quies}$ (Davenport 2016). The ED is the integral under the normalized K2 light curve during the flare. To calculate the energy released by the X-ray flares and the average plasma properties (plasma temperature: kT and emission measure [EM]), we have used XSPEC v. 12.8.1 (Arnaud 1996) to fit the X-ray spectrum of each source extracted during the flare with the astrophysical plasma emission code ionization-equilibrium isothermal plasma model (Smith et al. 2001). Results are summarized in Table 1.

Figure 5 shows the comparison between the total energy released in optical and in X-rays. As observed in most of the solar flares, the flares analyzed in this study typically released more energy in optical than in X-rays. As indicated by the two-sides Spearman test, the observed correlation between these quantities is weak. However, this is mainly due to the flares occurred in HCG 148 and HCG 244, for which the estimate of the X-ray flare duration is uncertain.

5 | TIME-RESOLVED SPECTRAL ANALYSIS

We studied the time evolution of the X-ray emitting plasma during the flares by sampling the MOS + PN light curves with suitable time intervals. We have calculated the time-resolved X-ray properties (plasma temperature and emission measure) repeating for each time interval

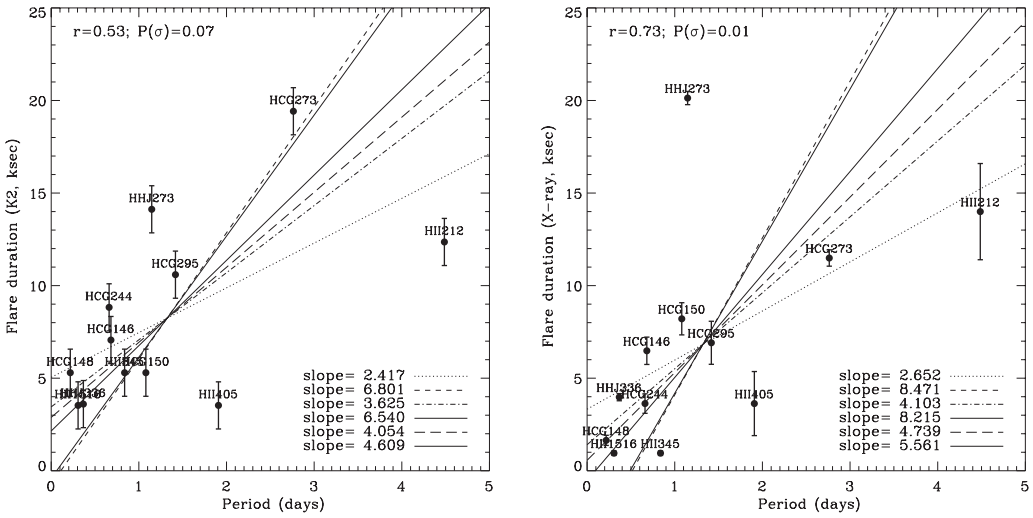

FIGURE 4 Flare duration in optical (left panel) and X-rays (right panel) vs. stellar rotation period. For each data point, we show the name of the star. The lines mark six linear fits performed with the *IDL* routine *SIXLIN*. The resulting slopes are indicated in the bottom right corner. In the top left corner we also show the Spearman's rank correlation coefficient and the significance of its deviation from zero. In both cases the most rapidly rotating stars in our sample host short flares

TABLE 1 Absorption, plasma temperature, luminosity, and total energy in optical and X-rays during quiescence and flares

Star	N_H (10^{21} cm^{-2})	kT_{quies} (keV)	kT_{flare} (keV)	$\log(L_{X\text{-}ray,quies})$ (erg s^{-1})	$\log(E_{X\text{-}ray,quies})$ (erg)	$\log(E_{kep,flare})$ (erg)
HII 212	0.6	$0.77^{0.85}_{0.69}$	$0.41^{0.63}_{0.33}$	$29.07^{29.12}_{29.02}$	$33.53^{33.57}_{33.40}$	34.17 ± 0.42
HHJ 273	1.2	$0.69^{0.77}_{0.62}$	$1.61^{1.70}_{1.52}$	$28.69^{28.73}_{28.64}$	$33.99^{34.02}_{33.97}$	34.08 ± 0.43
HHJ 336	1.1	$0.35^{0.42}_{0.29}$	$1.56^{1.65}_{1.45}$	$28.73^{28.80}_{28.65}$	$33.51^{33.54}_{33.48}$	33.45 ± 0.75
HCG 244	0.9	$0.58^{0.61}_{0.55}$	$1.66^{1.98}_{1.43}$	$29.10^{29.11}_{29.08}$	$32.89^{32.94}_{32.83}$	34.03 ± 0.42
HII 345	1.4	$0.59^{0.60}_{0.59}$	$2.45^{2.69}_{2.23}$	$30.18^{30.19}_{30.18}$	$33.68^{33.70}_{33.65}$	34.66 ± 0.51
HII 1516	0.2	$0.91^{0.93}_{0.89}$	$2.56^{3.21}_{2.30}$	$29.42^{29.43}_{29.41}$	$33.54^{33.57}_{33.51}$	33.71 ± 0.57
HCG 146	1.6	$0.74^{0.84}_{0.61}$	$0.78^{0.85}_{0.70}$	$28.53^{28.59}_{28.47}$	$32.98^{33.03}_{32.94}$	33.52 ± 0.48
HCG 273	1.1	$0.60^{0.64}_{0.56}$	$1.63^{1.69}_{1.57}$	$29.07^{29.09}_{29.05}$	$33.85^{33.86}_{33.83}$	34.33 ± 0.39
HCG 150	0.7	$0.61^{0.65}_{0.58}$	$2.16^{2.59}_{1.79}$	$28.96^{28.97}_{28.94}$	$33.07^{33.12}_{33.02}$	32.91 ± 0.53
HCG 295	0.7	$0.69^{0.76}_{0.62}$	$1.96^{3.22}_{1.44}$	$28.95^{28.98}_{28.91}$	$33.34^{33.45}_{33.24}$	33.48 ± 0.42
HII 405	1.0	$0.47^{0.49}_{0.46}$	$1.29^{1.36}_{1.21}$	$29.67^{29.68}_{29.65}$	$33.49^{33.52}_{33.46}$	33.89 ± 0.58
HCG 148	0.8	$0.32^{0.36}_{0.29}$	$1.00^{1.15}_{0.89}$	$28.67^{28.72}_{28.61}$	$33.02^{33.08}_{32.96}$	34.02 ± 0.51

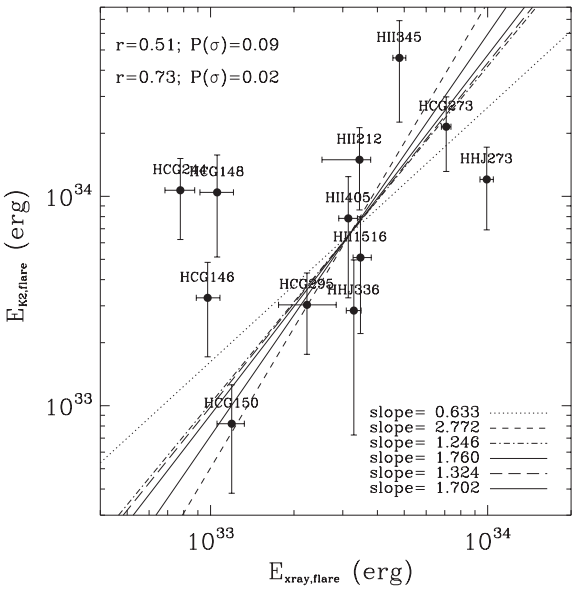

FIGURE 5 Comparison between the total energy emitted in optical and X-ray. The name of each star is also indicated. The lines mark six linear fits between the log values performed with the *IDL* routine *SIXLIN*. The resulting slopes are indicated in the top left corner. We also show the Spearman's rank correlation coefficient and the significance of its deviation from zero. These flares typically released more energy in optical than in X-rays

the spectral analysis described in section 4. The main objective of this analysis was to track the time evolution of the X-ray emitting plasma in the kT vs. log(EM) plane, because it can be used as diagnostic tool for flares cooling and heating processes (Reale 2007).

Figure 6 shows the time evolution of the flare observed in HCG 273.

For 10 stars in our sample, we have been able to calculate the slope of the cooling pattern (ζ) followed by the flares in the log(kT) vs. $0.5 \times \log(EM)$ plane by interpolating the points of the cooling phase. As shown by Jakimiec et al. (1992), Sylwester et al. (1993), and Reale et al. (1997), this value provides hints on the presence of heating during the cooling phase. In fact, ζ is expected to be $\sim$2 when negligible heating occurs during the cooling phase, otherwise it is <2. Despite suffering large uncertainties, the resulting slopes are compatible with the lack of substantial heating during the cooling phase in all the flares of our sample with the exception of HHJ 273 (with $\zeta = 0.4 \pm 1.1$) and HII 405 ($\zeta = 0.7 \pm 0.8$).

5.1 | Loop lengths

We estimated the size of the loops by applying relations between the loop size and observable quantities, which were derived by Reale et al. (1997) and Reale (2007) from hydrodynamic loop models. The first equation we used is:

$$L_{\rm loop} = 6 \times 10^{2.5} \times t_{\rm maxden} \times \Psi^2 \times T_{\rm max}^{0.5} \quad (1)$$

where t_{maxden} is the time from the flare onset at which the density reaches its peak, calculated as the difference between the half time of the interval with associated the largest emission measure and flare start; T_{max} is the maximum temperature, measured in K, calculated from the maximum temperature $T_{max,fit}$ obtained from the time-resolved spectral analysis using $T_{max} = 0.13 \times T^{1.16}_{max,fit}$ (specific for EPIC instruments, Reale 2007); ψ is the ratio between the peak temperature and the temperature at the density peak, which ranges between 1.2 and 2 (Reale 2007).

We also derived the loop lengths from the duration of the rise of the light curve (i.e., from the flare start to the peak of emission) t_{rise}, measured in ks. This duration is calculated from binned light curves and thus its value is affected by the uncertainty due to binning:

$$L_{\rm loop} = 0.6 \times \Psi^2 \times T_{\rm max}^{0.5} \times t_{\rm rise} \quad (2)$$

The median loop lengths are equal to 0.9 R_{star} using Equation (1) and 0.5 R_{star} using Equation (2).

5.2 | Oscillations

We have searched for oscillations in the X-ray flares using a wavelet analysis tool (López-Santiago 2018). This method is a modified version of the Fourier analysis designed to detect

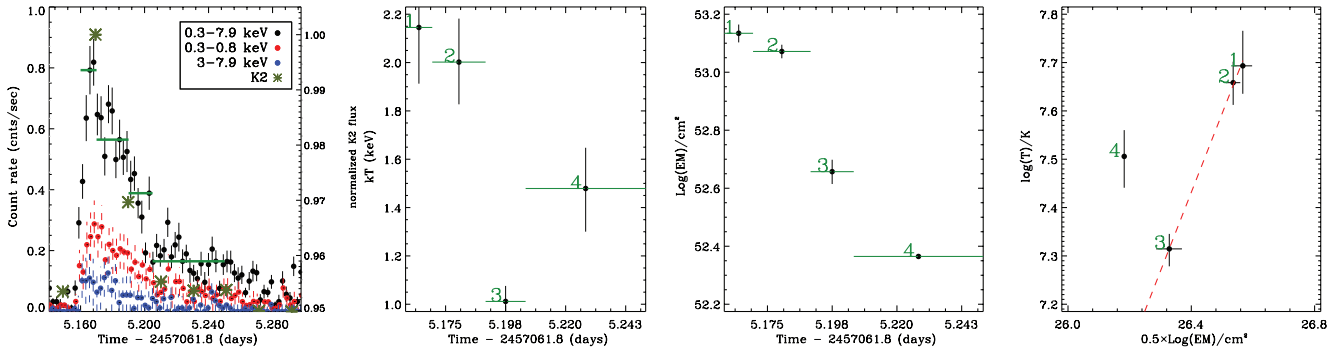

FIGURE 6 Evolution of the flare observed in HCG 273. The left panel shows the MOS + PN XMM light curve in three different energy bands (dots) superimposed on the K2 light curve (green asterisks). The horizontal green lines mark the defined time intervals. The central panels show the time evolution of plasma temperature and emission measure, while the right panel the evolution in the log(T) vs. 0.5 × log(EM) plane. The red dashed line marks the slope of the cooling phase

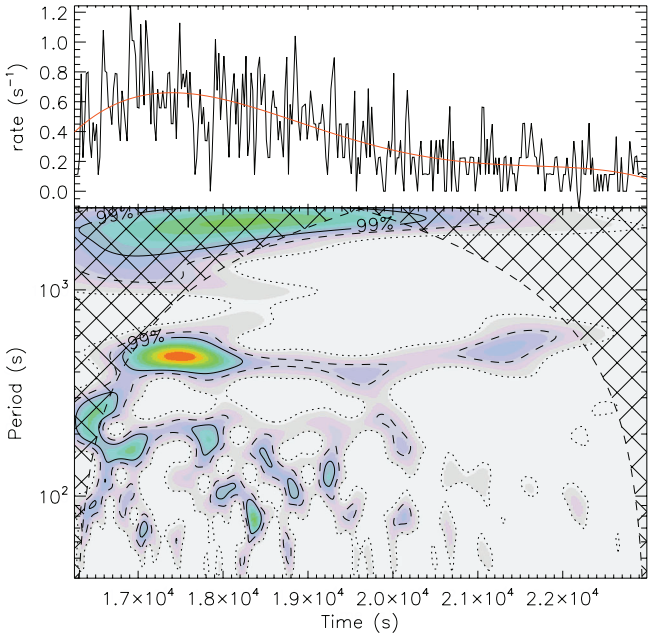

FIGURE 7 Bottom panel: wavelet power spectrum obtained during the flare in HCG 273, with contours marking peaks with 68, 95, and 99% confidence level. The hatched area is the "cone of influence" (see text). Top panel: observed light curve with overplotted the flare global shape. A significant oscillation with a period of 500 ± 100 s is detected

quasi-periodic signals, in which the light curve is transformed from time to frequency domain adopting a Morlet function as a mother function (Torrence & Compo 1998).

Figure 7 shows the wavelet power spectrum obtained from the flare in HCG 273, the only source in our sample for which we detected significant oscillations, with contours marking the peaks corresponding to 68, 95, and 99% confidence levels. The hatched area is the "cone of influence," which is the region of the power spectrum where the edge effects are important (Torrence & Compo 1998). A significant oscillation with a period of 500 ± 100 s is detected. The detection of oscillations in the flare observed in HCG 273 supports the hypothesis of a single loop dominating this flare, ignited by a single rapid heat pulses that are shorter than the sound crossing time across the loop at the maximum plasma temperature.

6 | CONCLUSIONS

We have analyzed 12 bright flares occurred in the Pleiades stars observed simultaneously with XMM/Newton and Kepler/K2, with the aim of calculating and comparing the energy released in the two bands and characterizing flares evolution and geometry. With a total energy released in the optical band in the $32.9 < \log(E_{kep,flare}) < 34.7$ range (median value 34.0, $E_{kep,flare}$ in erg), all the flares in our sample but one (the one occurred in HCG 150) meet the criteria for *superflares* defined by Shibayama et al. (2013) and Notsu et al. (2013) (e.g., $10^{33} \leq E_{optical} \leq 10^{38}$ erg). This is not surprising given that our sample is limited to bright flares occurring in young and rapidly rotating stars.

The flares observed in the Pleiades share some of the properties of the flares typically observed in the Sun, despite being more energetic. For instance, as in most of the solar flares, more energy is typically released in optical than in X-rays. Additionally, the energy budget in the two bands is weakly correlated. We also found that the flare duration in optical and X-rays is similar despite being typically longer in X-rays, and observed that rapidly rotating stars (e.g., with rotation period shorter than 0.5 days) preferentially host short flares. The time-resolved X-ray spectral analysis suggests that these flares are mainly due to single loops with no sustained heating occurring during the cooling phase. We also observed and analyzed oscillations with a period of 500 s during one of the flares.

REFERENCES

Albacete Colombo, J. F., Flaccomio, E., Micela, G., Sciortino, S., & Damiani, F. 2007, *A&A*, *464*, 211.

Argiroffi, C., Caramazza, M., Micela, G., Sciortino, S., Moraux, E., Bouvier, J., & Flaccomio, E. 2016, *A&A*, *589*, A113.

Arnaud, K. A. 1996, in: *Astronomical Data Analysis Software and Systems V*, eds. G. H. Jacoby & J. Barnes, SAO/NASA Astrophysics Data System, Vol. *101*, 17.

Benz, A. O. 2008, *Living Rev. Sol. Phys.*, *5*, 1.

Bouy, H., Bertin, E., Moraux, E., et al. 2013, *A&A*, *554*, A101.

Bouy, H., Bertin, E., Sarro, L. M., et al. 2015, *A&A*, *577*, A148.

Caramazza, M., Flaccomio, E., Micela, G., Reale, F., Wolk, S. J., & Feigelson, E. D. 2007, *A&A*, *471*, 645.

Damiani, F., Maggio, A., Micela, G., & Sciortino, S. 1997a, *ApJ*, *483*, 370.
Damiani, F., Maggio, A., Micela, G., & Sciortino, S. 1997b, *ApJ*, *483*, 350.
Davenport, J. R. A. 2016, *ApJ*, *829*, 23.
Fletcher, L., Dennis, B. R., Hudson, H. S., et al. 2011, *Space Sci. Rev.*, *159*, 19.
Gaia Collaboration, Brown, A. G. A., Vallenari, A., et al. 2016, *A&A*, *595*, A2.
Jakimiec, J., Sylwester, B., Sylwester, J., Serio, S., Peres, G., & Reale, F. 1992, *A&A*, *253*, 269.
López-Santiago, J. 2018, *Philos. Trans. R. Soc. Lond. A*, *376*, 20170253.
Notsu, Y., Shibayama, T., Maehara, H., et al. 2013, *ApJ*, *771*, 127.
Reale, F. 2007, *A&A*, *471*, 271.
Reale, F., Betta, R., Peres, G., Serio, S., & McTiernan, J. 1997, *A&A*, *325*, 782.
Rebull, L. M., Stauffer, J. R., Bouvier, J., et al. 2016, *AJ*, *152*, 113.
Scargle, J. D. 1982, *ApJ*, *263*, 835.
Shibayama, T., Maehara, H., Notsu, S., et al. 2013, *ApJS*, *209*, 5.
Smith, R. K., Brickhouse, N. S., Liedahl, D. A., & Raymond, J. C. 2001, *ApJ*, *556*, L91.
Stauffer, J. R., Schultz, G., & Kirkpatrick, J. D. 1998, *ApJ*, *499*, L199.
Sylwester, B., Sylwester, J., Serio, S., Reale, F., Bentley, R. D., & Fludra, A. 1993, *A&A*, *267*, 586.
Torrence, C., & Compo, G. P. 1998, *Bull. Am. Meteorol. Soc.*, *79*, 61.

How to cite this article: Guarcello MG, Argiroffi C, Drake JJ, et al. Simultaneous Kepler/K2 and XMM-Newton observations of superflares in the Pleiades. *Astron. Nachr.* 2019;340:302–307. https://doi.org/10.1002/asna.201913614